Biosensors and Bioelectronics 106 (2018) 99–104

Contents lists available at ScienceDirect

Biosensors and Bioelectronics

journal homepage: www.elsevier.com/locate/bios

Ultrasensitive label-free optical microfiber coupler biosensor for detection of cardiac troponin I based on interference turning point effect

Wenchao Zhou[a,1], Kaiwei Li[b,1], Youlian Wei[a,c], Peng Hao[a], Mingbo Chi[a], Yongshun Liu[a], Yihui Wu[a,*]

[a] State Key Laboratory of Applied Optics, Changchun Institute of Optics, Fine Mechanics and Physics, Chinese Academy of Sciences, Changchun 130033, PR China
[b] School of Electrical and Electronic Engineering, Nanyang Technological University, Singapore 639798, Singapore
[c] University of Chinese Academy of Sciences, Beijing 100039, PR China

ARTICLE INFO

Keywords:
Optical microfiber coupler
Biosensor
Dispersion turning point
Cardiac troponin I
Ultrasensitivity
Regeneration

ABSTRACT

Sensitive detection of cardiac biomarkers is critical for clinical diagnostics of myocardial infarction (MI) while such detection is quite challenging due to the ultra-low concentration of cardiac biomarkers. In this work, a label-free immunosensor based on optical microfiber coupler (OMC) has been developed for the ultrasensitive detection of cardiac troponin I (cTnI), a selective and highly sensitive biomarker of acute myocardial infarction (AMI). CTnI monoclonal antibodies were immobilized on the surface of the fiber through polyelectrolyte layer using layer-by-layer deposition technique. For refractive index sensing characterization, an ultra-high sensitivity of 91777.9 nm/RIU was achieved when the OMC works around the dispersion turning point, which is the highest experimental demonstration in the field of fiber-optic evanescent biosensors. For biosensing, the immunosensor with good specificity showed a linear wavelength shift in the range of 2–10 fg/mL and an ultra-low detection limit of 2 fg/mL. Such immunosensors have huge application potential for the detection of cardiac biomarkers of myocardial infarction due to simple detection scheme, quick response time, ease of handling and miniaturation.

1. Introduction

Myocardial infarction (MI), known as heart attack, is a major cause of morbidity and mortality worldwide. Data from World Health Organization (WHO) (Han et al., 2016) accounted 30% of global death annually and it is expected that more than 23 million die annually by 2030. Cardiac troponin I (cTnI) is considered as 'gold standard' biomarker for the detection of acute MI due to its remarkable specificity and sensitivity (Fathil et al., 2015). The levels of cTnI became a predominant diagnosis index for MI since it is usually produced only in the myocardium and shows high specificity to cardiac injury (Panteghini et al., 2004).

Conventional methods for monitoring the cTnI levels including enzyme linked immunesorbent assay (ELISA), radioimmunoassay (RIA) and high performance liquid chromatography (HPLC) (Bodor et al., 1992; Carraro et al., 1994; Neverova and Eyk, 2002), have suffered from some apparent problems such as long assay time, multistep processing, high overall cost and require sophisticated instrumentation. Therefore, it is difficult to apply those assays in developing countries or remote areas where diagnosis of AMI is urgently needed. Hence, a sensitive, rapid, and cost-efficient platform becomes an urgent demand to fulfill the diagnosis requirements in MI detection.

Meanwhile biosensors are now more acceptable because of their high sensitivity, reliability and point-of-care (POC) diagnosis. Over the past decades, various methodologies including colorimetric, fluorescence, paramagnetic, electrochemical etc. have been tested for cTnI detection (Han et al., 2016). Among the detection techniques, electrochemical approaches have been widely used due to their potential for the real-time monitoring of cTnI protein biomolecule interaction (Jo et al., 2015; Negahdary et al., 2017). Additionally, various commercially available cTnI detection instruments based on fluorescence assay can also be obtained for instance Roche Cardiac Reader, Abbott i-STAT and Singulex Erenna System etc. (Tate et al., 2012). However, the conjugation of labels with antibody or antigen requires long time and additional cost. Besides, the conjugation processes may reduce the bimolecular activities, which in turn decrease the sensitivity of the detection.

Nowadays, since increasing interest has been devoted to new methods of detecting and quantifying biomolecules because of their paramount importance to modern clinical and biological fields. Label-

* Corresponding author.
E-mail address: yihuiwu@ciomp.ac.cn (Y. Wu).
[1] These authors contributed equally to this work.

https://doi.org/10.1016/j.bios.2018.01.061
Received 18 October 2017; Received in revised form 16 January 2018; Accepted 29 January 2018
Available online 01 February 2018
0956-5663/

free bioassay technologies have attracted much attention in recent years due to its potential to address some of the limitations in other labeled methods. Label-free biosensors such as surface plasmon resonance (SPR) (Wu et al., 2017), quartz crystal microbalance (QCM) (Akter et al., 2015), surface acoustics wave (SAW) (Lee et al., 2013), photonics crystal (PC) (Zhang et al., 2014) and electrochemical impedance spectroscopy (EIS) (Akter et al., 2017) have potential for simplifying the molecular recognition process and enhancing the detection sensitivity. To further improve the sensitivity, many detection strategies based on nanomaterials have also been designed including graphene quantum dots (Tuteja et al., 2016), carbon nanofiber (Gupta et al., 2016; Periyakaruppan et al., 2013), silicon-nanowire (Kong et al., 2012; Kim et al., 2016.), carbon nanospheres (Gao et al., 2017), and znic oxide nanostructures (Shanmugam et al., 2017). However, synthesis, purification, fabrication and functionalization using those nanomaterials need some special treatments, skills and time.

Fiber-optic sensor can also work as label-free biosensors. However, most of the proposed fiber-optic biosensors suffer from relatively low sensitivity for both refractive index (RI) sensing and biosensing (Sun et al., 2014; Liu and Li, 2015; Zhang et al., 2016; Chiavaioli et al., 2014; Liu et al., 2017). Recently we proposed and studied an optical microfiber coupler(OMC) sensor working near the turning point of effective group index difference between the even supermode and odd supermode to achieve high RI sensitivity. Infinite sensitivity can be obtained when the dimension of the OMC is close to the turning point value. Ultrahigh sensitivity of 39541.7 nm/RIU, which is at least one order higher than other optical RI sensors, was experimentally demonstrated using an OMC with diameter of 1.4 μm (Li et al., 2016). In this study, an ultrasensitive label-free fiber biosensor based on this micro-fiber coupler with high reproducibility was proposed to detect cardiac troponin I. Ultrasensitivity can be achieved when the wavelength peak shift works around the turning point. A detection limit of 2 fg/mL in phosphate buffer saline (PBS, pH7.4) buffer was obtained, which is the lowest limit for fiber-optic biosensors to the best of our knowledge. Besides, this biosensor exhibited a linear optical response to cTnI over the concentration range of 2–10 fg/mL in PBS buffer. The results suggested that the proposed immunosensor is a useful tool for practical application in clinical diagnosis.

2. Material and methods

2.1. Reagents and materials

Single-mode optical fiber with core and cladding diameters of 8 μm and 125 μm was purchased from Corning Inc. (New York, USA). Potassium hydroxide (KOH) was obtained from Sinopharm Chemical Reagent Co.,Ltd (Shanghai China). Poly-(diallyldimethylammonium chloride) (PDDA), poly-(acrylic acid) (PAA), N-Hydroxysuccinimide (NHS), 1-(3-Dimethylaminopropyl)−3- ethalcarbodimide hydrochloride(EDC), Phosphate buffer saline(PBS) and bovine serum albumin (BSA) were purchased from Sigma-Aldrich(St. Louis,USA). The cardiac troponin I antigens and monoclonal cTnI antibodies were supplied from Wondofo Biomedical Co., Ltd(Guangzhou,China). Prostate specific antigen (PSA), C-reaction protein (CRP), Immunoglobulin G (IgG) were purchased from Biosynthesis Biotechnology Co., Ltd (Beijing, China). All the chemical reagents were of analytical grade. All solutions were prepared using deionized water (18.2MΩcm) obtained from a MilliQ filtration system (Millipore, USA).

2.2. Experimental setup

The experimental setup is shown in Fig. 1(a). A halogen lamp was used as the light source and the light was focused into the fiber using a microscope objective with numerical aperture of 0.65. An optical microfiber coupler was fixed in a fluid cell and the cell was integrated with a polydimethylsiloxane (PDMS) chamber for delivery of sample solutions. A spectrometer with a resolution of 0.3 nm was used as the detector and the data were acquired by a laptop. To eliminate the influence of temperature, the biosensing experiments were carried out in a clean room environment and the temperature of 23 ± 0.2 ℃ was maintained whole through the experiments.

2.3. Preparation of optical fiber coupler biosensor

OMC was prepared by the fusion elongation method (Yokohama et al., 1987; Xu et al., 2017). Our thermal pulling system consists of three stages, three electric motors, two fiber clamps, a hydrogen generator, an oxyhydrogen torch and a control panel. Two bare optical fibers are double twisted, along in parallel and fixed on the elongation stages. The oxyhydrogen torch was used to heat the fibers and the flow rate can be controlled by the hydrogen generator. Two electric motors can pull the fiber in opposite direction. To get uniform couplers, the flame was scanned by another motor and the length of the uniform waist can be controlled by the distance of the scanning. The pulling process was monitored by an online monitoring system and the waist diameters of the OMC can be controlled precisely by monitoring the output power. In our experiments, the pulling speed can be controlled in 4 mm/min, and the hydrogen gas flow rate was 90 mL/min with the purity of 99.999%. To keep the coupler stable and robust, they were placed in fluid cells and fixed by PDMS. The fluid cells were fabricated on PMMA plates using laser writing technology. Typical images of the chip and the fabricated fiber coupler are depicted in Fig. 1(b).

2.4. Immobilization of antibodies on the biosensor surface

The immobilization of antibody on the OMC surface and the biodetection process are depicted in Fig. 1(c). Prior to the functionalization the biosensor chips were cleaned with deionized H_2O (18 MΩ) and then the samples were immersed in 0.1 M KOH solution for 10 min to create hydroxyl(-OH) groups on the surface (Baranowska et al., 2015; Kim and Herr, 2013). The surfaces were then washed with distilled water. Next the fiber biosensor surface was prepared by alternating incubation for 30 mins with 2 mg/mL PDDA (positively charged) and 2 mg/mL PAA (negatively charged) to get final modification with individually spotted capture proteins (Yuk et al., 2013). The surfaces were also washed with deionized H_2O (18 MΩ). To facilitate capture protein binding, the carboxyl group of PAA was activated to form reactive NHS using a solution of 50 mM NHS and 200 mM EDC in water for 30 min. Blocking to reduce subsequent non-specific binding was then performed by incubating the sensor chip surface with a blocking solution (3% BSA in the PBS, pH7.4) for 30 mins. The biosensor chip was then washed with PBS for 5 mins. Subsequently, functionalized fiber was incubated with cTnI antibody with concentration of 100 μg/mL for 1 h to immobilize the antibody to fiber surface. Alongside, various concentrations of cTnI (2 fg/mL to 10 fg/mL with a step of 2 fg/mL) proteins solutions were prepared by dilution with PBS in advance.

2.5. Detection mechanism of the biosensor

Fiber coupler has a wide a range of uses in the optical networking industry, for example power splitters, wavelength-division multiplexers, mode splitters etc. Power exchange occurs as the even and odd supermodes propagate along the OMC and thus an interferometric spectrum is obtained at the output ports as shown in Fig. 2(a). According to the supermode theory, the output powers at through port P3 and cross port P4 are then given by

$$P_3 = P_1 \cos^2\left(\frac{1}{2}\phi\right), \quad P_4 = P_1 \sin^2\left(\frac{1}{2}\phi\right) \tag{1}$$

where ϕ represents the phase difference between the two supermodes accumulated along the coupling region for TE/TM polarization.

We described the phase term as that a uniform OMC and take a

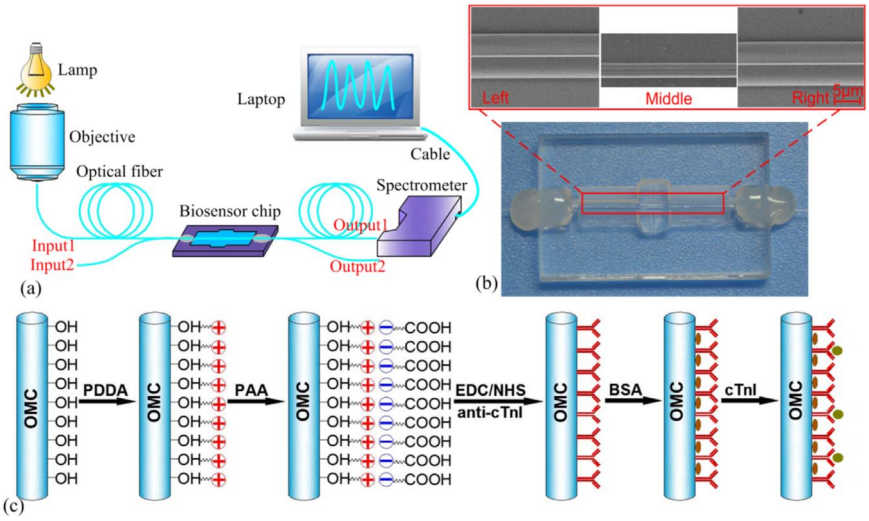

Fig. 1. (a) Illustration of the experimental setup, (b) Image of the biosensor cell and of a 1.0 μm thick optical microfiber coupler, (c) Schematic illustration of fiber optic biosensor based on OMC structure.

small variation in theory, the spectral dependency on the external RI is obtained as (Li et al., 2016)

$$S = \frac{\partial \lambda_N}{\partial n} = \frac{\lambda_N}{\Delta n_{eff} - \lambda_N \partial(\Delta n_{eff})/\partial\lambda} \frac{\partial(\Delta n_{eff})}{\partial n} \quad (2)$$

where Δ_{neff} represents the effective RI difference between the two supermodes and $G = \Delta_{neff} - \lambda_N \partial(\Delta_{neff}) / \partial\lambda$ is defined as the group effective index difference between even and odd supermodes for TE/TM polarization. And the RI sensitivity can reach infinity when $G = 0$, which is corresponding to the turning point. The surrounding RI is usually modified by biomolecules adsorbed on the fiber surface (Vörös, 2004; Ball and Ramsden, 1998; Zhao et al., 2011), so OMC have the potential to work as a biosensor.

3. Results and discussion

3.1. Numerical simulations and RI sensing characteristics

In order to obtain good performance, the dimension of the OMC should be carefully designed. The sensitivity for OMC with different diameters in water environment was calculated. The results illustrated in Fig. 2(b) shows distinctive turning point at the wavelength range of 650–1300 nm when the diameter of the OMC reduces below 1.2 μm. When the OMC sensor works near the turning point, the effective RI of the odd mode is very close to the RI of water, and a large quantity of the guided power in the odd mode will be exposed into the surrounding medium in the form of evanescent wave. Thus, the strength of light-matter interaction was significantly enhanced and the RI sensitivity would be greatly improved. Considering the spectra range of our light source is 450–980 nm, we use an OMC with a diameter of about 0.7 μm for the RI sensing characterization. The response of the OMC in solution with different RI was tested by tracing the shifting of peaks in the transmission spectrum. The liquid we used was the mixture of the glycerol and deionized water. The range of this solution was from 1.33300 to 1.33320 with a step of 0.00004. As demonstrated in Fig. 3, the peaks redshift dramatically with increase of the RI around the turning point. The RI sensitivity is higher for long wavelength than for short wavelength. Moreover, an ultrasensitivity of 91777.9 nm/RIU is achieved near the turning point, which is so far the highest sensitivity for OMC based sensors at low RI around 1.33. The reproducibility can be evaluated in terms of relative standard deviation(RSD) with a maximum for each point of 8.1% (n = 5). Besides, we plot the sensitivity in our experiment together with numerialcal simulations results in the inset of Fig. 3(b), and our experimental results agree well with the theoretical results. The small discrepancy could be attributed to the fact that the actual OMC geometry is not a perfect uniform parallel cylinder compared with the theoretical model.

Although the sensitivity of our sensor is very high, the dynamic range is relatively narrow. A feasible method to broaden the dynamic range is to reduce the coupling length L, which eventually would enlarge the period of oscillation in the output spectrum. However, it will also lead to a decrease to the quality factor of the interference peaks. The trade-off between quality factor and dynamic range should be considered when the OMC based RI sensor is applied to different

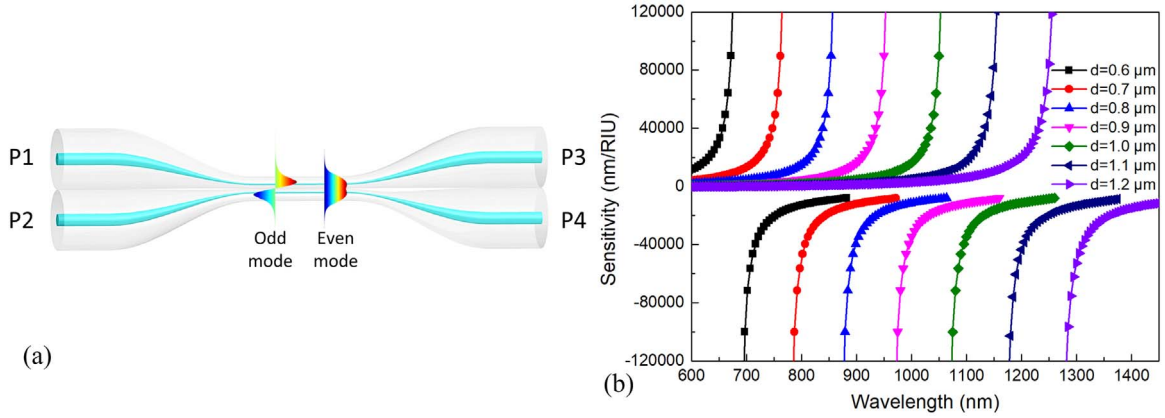

Fig. 2. (a) Schematic diagram of the microfiber coupler with even mode and odd mode, (b) Modeled sensitivity versus wavelengths at the turning point with different diameters (0.6–1.2 μm).

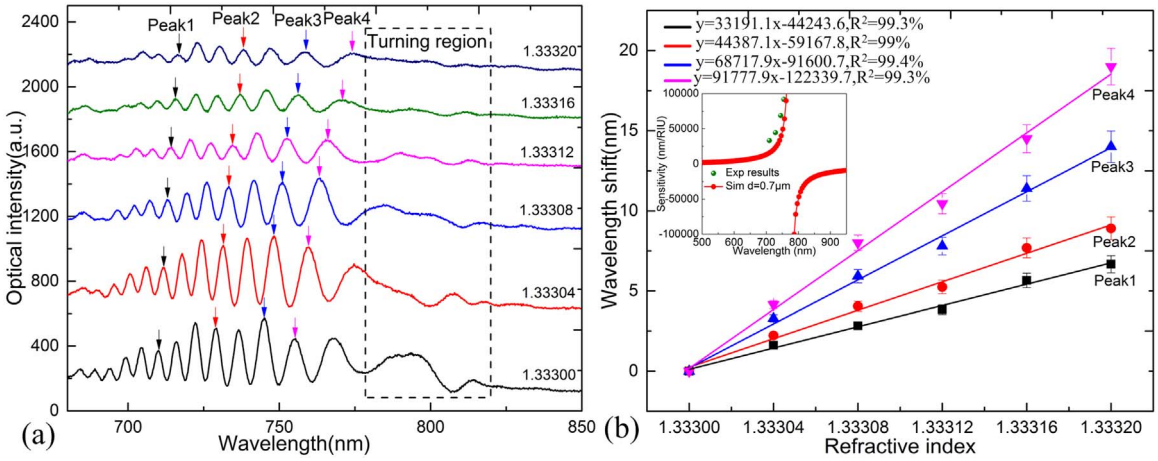

Fig. 3. (a) Transmission spectral responses to different ambient RIs of 1.33300, 1.33304, 1.33308, 1.33312, 1.33316, and 1.33320. Black, red, blue and magenta arrows are to guide the shift of interference peaks as ambient RI increases (The spectra are offset for clarity). (b) Wavelength peaks shift corresponding to different peaks indicted by the different arrows versus different ambient RIs. Inset: simulated (red) and experimental results (olive) of sensitivity versus wavelength.

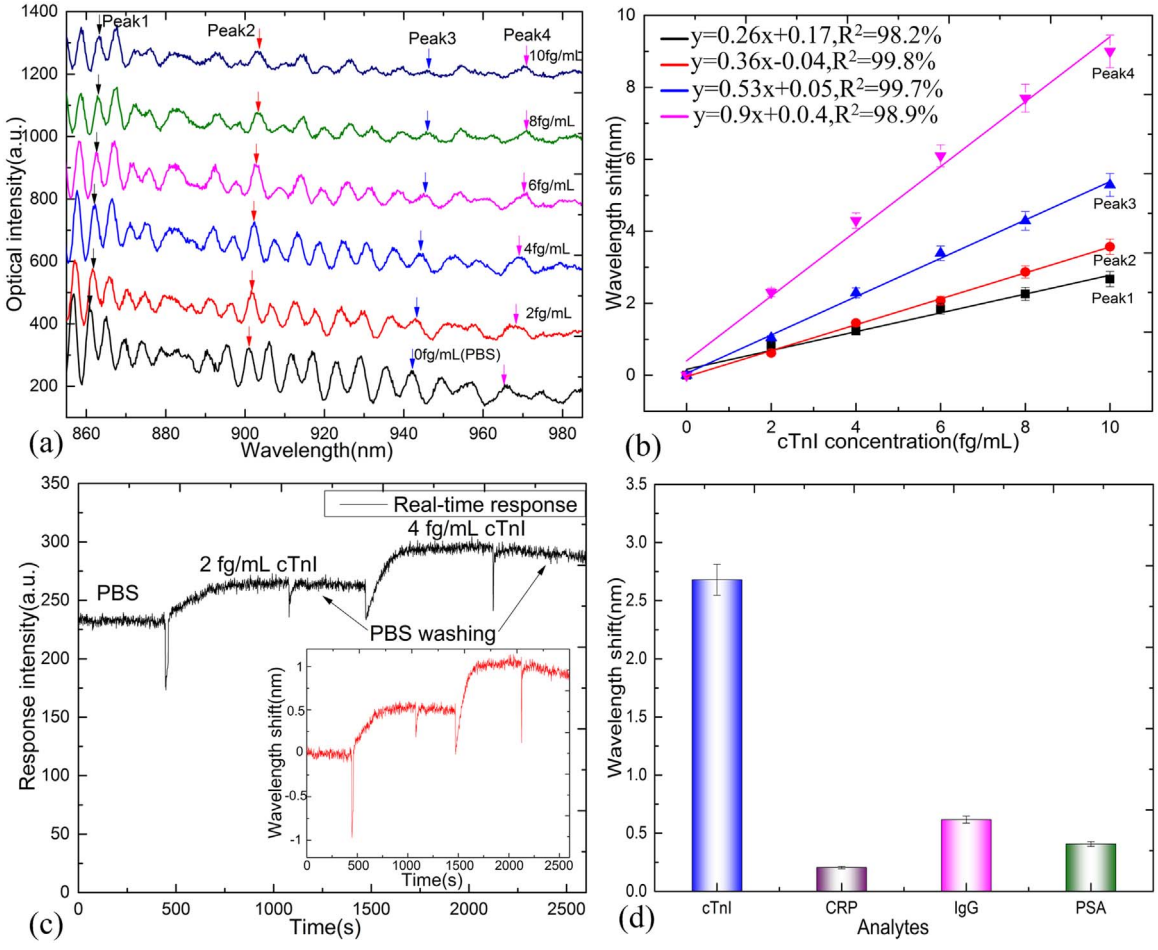

Fig. 4. (a) Transmission spectral responses near the turning point of effective group index difference (The spectra are offset for clarity), (b) Peak wavelength shift with different concentrations of cTnI (PBS, 2 fg/mL, 4 fg/mL,6 fg/mL,8 fg/mL,10 fg/mL respectively), (c) Real-time response transmission spectrum with PBS, 2fg/mL and 4fg/mL , inset: corresponding wavelength shift.(d) Measured response to cTnI antigen and other non-specific protein (CRP, IgG, PSA) with the same concentration of 10 fg/mL in PBS buffer.

occasions.

3.2. Detection of cTnI in PBS buffer and specificity

The OMC could be extremely sensitive to biomolecules binding to the sensor surface. To explore the performance of this ultrasensitive OMC biosensor, detection of cTnI in PBS buffer was carried out. Here we used an OMC with a diameter of 1 μm for our experiments considering sub-micro-sized OMCs are too fragile to go through the chemical modification for antibody immobilization. cTnI antibody-antigen binding was performed by injecting and incubating 100 μL of cTnI solution in PBS with concentration ranging from 2 fg/mL to 10 fg/mL at room temperature for around 10 min Fig. 4(a) shows the typical transmission spectral response of the OMC biosensor. Interference

Table 1
Comparison of the limit of detection for cTnI biosensors.

Methods	Media	Limit of detection	Reference
OMC sensor	PBS	2fg/mL	Present work
Optical SIS sensor	PBS	5 pg/mL	Diware et al. (2017).
Electrochemiluminescent	Serum	0.08 pg/mL	Zhou et al. (2014).
Field effect transistor(FET)	PBS	1 pg/mL	Tuteja et al. (2014).
Electrochemical	PBS	4.2 pg/mL	Singal et al. (2014).
Electrochemical	PBS	24 pg/mL	Jo et al. (2015).
Electrochemical	Serum	1 pg/mL	Shanmugam et al. (2017).
Electrochemical	PBS	8 pg/mL	Negahdary et al. (2017).
FET-based In_2O_3 nanoribbon	PBS	1 pg/mL	Liu et al. (2016a).
Colorimetric assay	Serum	0.2 ng/mL	Liu, . et al. (2016b)
ELISA	PBS	5 pg/mL	Zhang et al. (2015).
Photoelectrochemical	Serum	1.756 pg/mL	Tan et al. (2017).
Silicon nanowire FET	PBS	5 pg/mL	Kim et al. (2016).
Silicon nanowire FET	PBS	0.092 ng/mL	Kong et al. (2012).
Surface plasmon resonance	PBS	1.25 ng/mL	Wu et al. (2017).
Surface acoustic wave(SAW)	Serum	6.2 pg/mL	Lee et al. (2013).
Photonic crystal	PBS	0.1 ng/mL	Zhang et al. (2014).
Electrochemical impedance spectroscopy	Serum	1 pg/mL	Akter et al. (2017).
Carbon nanofiber nanoelectrode array	PBS	0.2 ng/mL	Periyakaruppan et al. (2013).
Optical point-of-care immunoassay	Serum	0.22 ng/mL	Rodenko et al. (2017).
Fluorescence	Serum	0.002 ng/mL	Seo et al. (2016).

between the even mode and odd mode can be observed for the whole wavelength range. Due to the limitation of our spectrometer, the spectrums beyond 980 nm were not measured, so the turning point which theoretically exists at around 1050 nm could not be observed. Even though, from the fast expansion of the free spectral range (FSR) as the wavelength red shifts, we can infer that the wavelength range of 850–980 nm is already very close to the turning point. Furthermore, the sensitivity increases dramatically when the peaks redshifts, as shown in the theoretical results in Fig. 2(b).

By comparing the spectra for different cTnl concentrations, we can clearly find that all the peaks tend to redshift as the concentration increases from 2 fg/mL to 8 fg/mL. This is caused by the binding of the cTnl molecules which can lead to small increases to the surrounding RI. The wavelength shifts of four typical peaks from short wavelength to long wavelength are depicted in Fig. 4(b). It is very obvious that the sensitivity improves rapidly as the peak wavelength increases. This fast increase phenomenon in the sensitivity is consistent with the behavior for RI sensing as predicted by the theoretical results in Fig. 2(b). As illustrated in Fig. 4(b), the maximum of RSD for cTnI in PBS buffer is about 8.39% (n = 5). More importantly, by utilizing the turning point, an ultra-low detection limit of 2 fg/mL and good linearity in the concentration rang of 2–8 fg/mL for cTnl is achieved, which is beneficial to the immunosensor in product.

To further show the dynamic process, the real-time response to cTnI with concentrations of 2 fg/mL and 4 fg/mL cTnI have been obtained by monitoring the output intensity at wavelength 904 nm as shown in Fig. 4(c). The optical intensity gradually increases when cTnI was injected compared to PBS. Then the optical intensity reached a plateau due to saturation effect which can be considered a complete antibody-antigen conjugation process. The corresponding wavelength shift was demonstrated in the inset of Fig. 4(c).

Table 1 summarizes the limit of detection of cTnI biosensor from this work and previous reports in literatures. The present OMC biosensor has the lowest limit in the PBS medium to date.

The specificity of this OMC biosensor was assessed by measuring three-kinds of non-specific proteins CRP, IgG and PSA. These proteins were diluted in the PBS with the same concentration of 10 fg/mL. From the test results illustrated in Fig. 4(d), the proposed sensor responded lower for all the three kinds of non-specific proteins, demonstrating its high specificity.

3.3. Regeneration of the sensor

Regeneration and reusability are important characteristics for biosensors. To investigate the regeneration of this biosensor, real-time monitoring of cTnI antigen binding to the cTnI antibody was conducted, and a mild regeneration reagent of 0.1 M glycine-HCl buffer (pH2.3) was used to dissociate the captured antigen-antibody complex similar to our previous work (Li et al., 2014). After each immune response, the regeneration step was carried out by short injections of the regeneration buffer with 1–3 min. As shown in Fig. 5, the output light intensity returned to the initial level after each regeneration cycle. And this biosensor can be reused for at least 8 cycles without significant losses in sensitivity, indicating the good stability of the immunosensor.

4. Conclusions

In this work, we have proposed an ultrasensitive label-free OMC biosensor for the detection of cardiac troponin I. The RI sensing performance of OMC based sensors around the turning point of the effective group index difference between even and odd supermodes was presented. An ultrasensitivity of 91777.9 nm/RIU at a low ambient RI

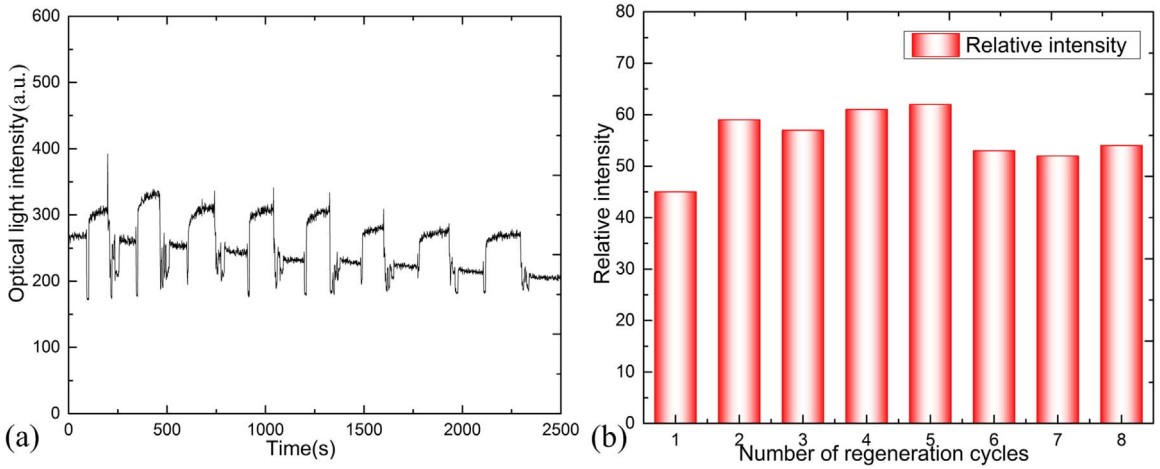

Fig. 5. (a) Real-time response curves for the sensor after a number of regeneration cycles. (b) The sum up of the biosensor response for each cycle with relative optical intensity (the reaction optical intensity subtracts the initial intensity).

of 1.33300 using a 0.7 μm thick OMC is experimentally demonstrated. A detection limit as low as 2 fg/mL for cTnI protein in PBS buffer was achieved around the turning point of the coupler where the sensitivity improved rapidly. Additionally, linear wavelength shift was obtained in the range of 2–10 fg/mL for all of the four typical peaks. By monitoring the wavelength shift or optical intensity at a selected wavelength, the real time responses of the antibody-antigen conjugation process were also obtained for low cTnI concentrations of 2 fg/mL and 4 fg/mL. Besides, non-specific proteins (CRP, IgG, and PSA) were adopted to certify the specificity of the biosensor. Furthermore, the regeneration characteristics were investigated and the results show that OMC biosensor can be reused for at least 8 cycles without significant loss in sensitivity. It is expected that this novel biosensor can serve as a necessary step towards potential applications for fast and accurate quantification of cTnI concentrations in blood samples from patients in clinical settings. Besides, for the point of care analysis, the proposed biosensor strategy could also be used for the detection of other protein biomarkers by only changing the appropriate antibody on the OMC surface. In future work, this OMC biosensor will be applied in the human serum samples, which is essential in POC testing applications.

Acknowledgements

This work was supported by the China-Israel International Science and Technology Cooperation Program (2015DFG02620), Natural Science Foundation of China (61504143,51505456, 61727813), National High Technology Development Program of China (2015AA042402) and the Technology Development Program of Jilin province (20170414015GH, 20160520097JH). The authors gratefully acknowledge Pinkie Eravuchira in Tel Aviv University for useful discussions.

References

Akter, R., Jeong, B., Lee, Y.M., Choi, J.S., Rahman, M.A., 2017. Biosens. Bioelectron. 91, 637–643.
Akter, R., Rhee, C.K., Rahman, M.A., 2015. Biosens. Bioelectron. 66, 539–546.
Baranowska, M., Slota, A.J., Eravuchira, P.J., Alba, M., Formentin, P., Pallarès, J., Ferré-Borrull, J., Marsal, L.F., 2015. J. Colloid Interface Sci. 452, 180–189.
Ball, V., Ramsden, J.J., 1998. Biopolymers 46, 489–492.
Bodor, G.S., Porter, S., Landt, Y., Ladenson, J.H., 1992. Clin. Chem. 38, 2203–2214.
Carraro, P., Plebani, M., Varagnolo, M.C., Zaninotto, M., Rossetti, M., Burlina, A., 1994. J. Clin. Lab. Anal. 8, 70–75.
Chiavaioli, F., Biswas, P., Trono, C., Bandyopadhyay, S., Giannetti, A., Tombelli, S., Basumallick, N., Dasgupta, K., Baldini, F., 2014. Biosens. Bioelectron. 60, 305–310.
Diware, M.S., Cho, H.M., Chegal, W., Cho, Y.J., Kim, D.S., O, S.W., Kim, K.S., Paek, S.H., 2017. Biosens. Bioelectron. 87, 242–248.
Fathil, M.F.M., Arshad, M.K.M., Gopinath, S.C.B., Hashim, U., Adzhri, R., Ayub, R.M., Ruslinda, A.R., Nuzaihan, M.N., M., Azman, A.H., Zaki, M., Tang, T.H., 2015. Biosens. Bioelectron. 70, 209–220.
Gao, H., Wen, L., Wu, Y., Fu, Z., Wu, G., 2017. Biosens. Bioelectron. 97, 122–127.
Gupta, R.K., Pandya, R., Sieffert, T., Meyyappan, M., Koehne, J.E., 2016. J. Electroanal. Chem. 773, 53–62.
Han, X., Li, S., Peng, Z., Othman, A.M., Leblanc, R., 2016. ACS Sens. 1, 106–114.
Jo, H., Gu, H., Jeon, W., Youn, H., Her, J., Kim, S.K., Lee, J., Shin, J.H., Ban, C., 2015. Anal. Chem. 87, 9869–9875.
Tate, J., Barth. J., Bunk,D., 2012. Analytical characteristics of commercial and research cardiac troponin I and T assays declared by the manufacturer; 〈http://www.ifcc.org/media/218177/IFCC%20Troponin%20Tables%20ng_L%20Update_December%202012.pdf〉.
Kim, D., Herr, A.E., 2013. Biomicrofluidics 7, 041501.
Kim, K., Park, C., Kwon, D., Kim, D., Meyyappan, M., Jeon, S., Lee, J.S., 2016. Biosens. Bioelectron. 77, 695–701.
Kong, T., Su, R., Zhang, B., Zhang, Q., Cheng, G., 2012. Biosens. Bioelectron. 34, 267–272.
Lee, J., Lee, Y., Park, J.Y., Seo, H., Lee, T., Lee, W., Kim, S.K., Hahn, Y.K., Jung, J., Kim, S., Choi, Y.S., Lee, S.S., 2013. Sens. Actuators B-Chem. 178, 19–25.
Li, K., Liu, G., Wu, Y., Hao, P., Zhou, W., Zhang, Z., 2014. Talanta 120, 419–424.
Li, K., Zhang, T., Liu, G., Zhang, N., Zhang, M., Wei, L., 2016. Appl. Phys. Lett. 109, 101101.
Liu, C., Cai, Q., Xu, B., Zhu, W., Zhang, L., Zhao, J., Chen, X., 2017. Biosens. Bioelectron. 94, 200–206.
Liu, G., Li, K., 2015. Sens. Actuators B-Chem. 215 (164-151).
Liu, Q., Aroonyadet, N., Song, Y., Wang, X., Cao, X., Liu, Y., Cong, S., Wu, F., Thompson, M.E., Zhou, C., 2016a. ACS Nano 10, 10117–10125.
Liu, X., Wang, Y., Chen, P., McCadden, A., Palaniappan, A., Zhang, J., Liedberg, B., 2016b. ACS Sens. 1, 1416–1422.
Negahdary, M., Behjati-Ardakani, M., Sattarahmady, N., Yadegari, H., Heli, H., 2017. Sens. Actuators B-Chem. 252, 62–71.
Neverova, I., Eyk, J.E.V., 2002. Proteomics 2, 22–31.
Panteghini, M., Pagani, F., Yeo, K.T.J., Apple, F.S., Christenson, R.H., Dati, F., Mair, J., Ravkilde, J., Wu, A.H.B., 2004. Clin. Chem. 50, 327–332.
Periyakaruppan, A., Gandhiraman, R.P., Meyyappan, M., Koehne, J.E., 2013. Anal. Chem. 85, 3858–3863.
Rodenko, O., Eriksson, S., Lichtenberg, P.T., Troldrorg, C.P., Fodgaard, H., Os, S., Pedersen, C., 2017. Biomed. Opt. Express 8, 3749–3762.
Shanmugam, N.R., Muthukumar, S., Chaudhry, S., Anguiano, J., Prasad, S., 2017. Biosens. Bioelectron. 89, 764–772.
Seo, S.M., Kim, S.W., Park, J.N., Cho, J.H., Kim, H.S., Paek, S.H., 2016. Biosens. Bioelectron. 83, 19–26.
Singal, S., Srivastava, A.K., Biradar, A.M., Mulchandani, A., Rajesh, 2014. Sens. Actuators B-Chem. 205, 363–370.
Sun, D., Guo, T., Ran, Y., Huang, Y., Guan, B.O., 2014. Biosens. Bioelectron. 61, 541–546.
Tan, Y., Wang, Y., Li, M., Ye, X., Wu, T., Li, C., 2017. Biosens. Bioelectron. 97, 741–746.
Tuteja, S.K., Chen, R., Kukkar, M., Song, C.K., Mutreja, R., Singh, S., Paul, A.K., Lee, H., Kim, K.H., Deep, A., Suri, C.R., 2016. Biosens. Bioelectron. 86, 548–556.
Tuteja, S.K., Sabherwal, P., Deep, A., Rastogi, R., Paul, A.K., Suri, C.R., 2014. ACS Appl. Mater. Interfaces 6, 14767–14771.
Vörös, J., 2004. Biophys. J. 87, 553–561.
Wu, Q., Sun, Y., Zhang, D., Li, S., Zhang, Y., Ma, P., Yu, Y., Wang, X., Song, D., 2017. Biosens. Bioelectron. 96, 288–293.
Xu, Y., Fang, W., Tong, L., 2017. Opt. Express 9, 10434–10440.
Yokohama, I., Noda, J., Okamoto, K., 1987. J. Light. Technol. 7, 910–915.
Yuk, J.S., Guignon, E.F., Lynes, M.A., 2013. Analyst 138, 2576–2582.
Zhang, B., Morales, A.W., Peterson, R., Tang, L., Ye, J.Y., 2014. Biosens. Bioelectron. 58, 107–113.
Zhang, Q., Prabhu, A., San, A., Al-Sharab, J.F., Levon, K., 2015. Biosens. Bioelectron. 72, 100–106.
Zhang, M., Li, K., Shum, P.P., Yu, X., Zeng, S., Wu, Z., Wei, L., 2016. In CLEO: Science and Innovations, SM4P-4.
Zhao, H.Y., Brown, P.H., Schuck, P., 2011. Biophys. J. 100, 2309–2317.
Zhou, Y., Zhuo, Y., Liao, N., Chai, Y., Yuan, R., 2014. Talanta 129, 219–226.